

Provided for non-commercial research and education use.
Not for reproduction, distribution or commercial use.



This article appeared in a journal published by Elsevier. The attached copy is furnished to the author for internal non-commercial research and education use, including for instruction at the authors institution and sharing with colleagues.

Other uses, including reproduction and distribution, or selling or licensing copies, or posting to personal, institutional or third party websites are prohibited.

In most cases authors are permitted to post their version of the article (e.g. in Word or Tex form) to their personal website or institutional repository. Authors requiring further information regarding Elsevier's archiving and manuscript policies are encouraged to visit:

<http://www.elsevier.com/authorsrights>

Available online at www.sciencedirect.com
SciVerse ScienceDirect
journal homepage: www.elsevier.com/locate/acme

Original Research Article

Phase transitions in metallic alloys driven by the high pressure torsion


 B. Straumal^{a,b}, A. Korneva^{c,*}, P. Zięba^c
^aInstitute of Solid State Physics, Russian Academy of Sciences, Ac. Ossipyan Str. 2, 142432 Chernogolovka, Russia

^bLaboratory of Hybrid Materials, National University of Science and Technology, MISIS, Leninskii prosp. 4, 119049 Moscow, Russia

^cInstitute of Metallurgy and Materials Science, Polish Academy of Sciences, Reymonta St. 25, 30-059 Cracow, Poland

ARTICLE INFO

Article history:

Received 25 March 2013

Accepted 4 July 2013

Available online 10 July 2013

Keywords:

Severe plastic deformation

Phase transformations

High-pressure torsion

Effective temperature

ABSTRACT

Severe plastic deformation can lead to the phase transformations in the materials. Even the severe plastic deformation at ambient temperature is frequently equivalent to the heat treatment at a certain elevated temperature (effective temperature). However, if the real annealing at the elevated temperature leads to the grain growth, the severe plastic deformation leads to strong grain refinement. In this review the methods of determination of effective temperature after high-pressure torsion of metallic alloys are discussed.

© 2013 Politechnika Wroclawska. Published by Elsevier Urban & Partner Sp. z o.o. All rights reserved.

1. Introduction

Severe plastic deformation (SPD) frequently leads to the phase transformations in the materials. Even the SPD-treatment at ambient temperature $T_{SPD}=300$ K is frequently equivalent to the heat treatment at a certain elevated temperature $T_{eff}>300$ K. It has been demonstrated recently that concept of effective temperature T_{eff} originally proposed for the materials under severe irradiation [1] is applicable also for severe plastic deformation (SPD) [2]. If the atomic movements driven by an external action (deformation or irradiation) are higher in comparison with the conventional thermal diffusion, the material is forced to undergo into a state which is equivalent to that at a certain increased (effective) temperature T_{eff} . One can estimate T_{eff} if the phases in a material after SPD treatment differ from those before SPD [2]. This method is quite

productive since SPD frequently leads to the phase transformations [3] e.g. the formation [4–12] or decomposition [13–15] of a supersaturated solid solution, dissolution of phases [16–28], disordering of ordered phases [19–31], amorphization of crystalline phases [32–40], synthesis of the low-temperature [21,28], high-temperature [41–43] or high-pressure [44–52] allotropic modifications, and nanocrystallization in the amorphous matrix [53–61]. For the determination of T_{eff} one can use also the phase diagrams at high pressures, if they are known [44–52]. However, the SPD-treatment at ambient temperature T_{SPD} usually leads to the very quick phase transformations, which is easy to understand if one considers the high density of defects, similar to an increased temperature. The increased pressure, oppositely, leads to the decrease of diffusivity and/or grain boundary mobility [62,63]. Some SPD-driven phase transformation needs only a small shift of atoms, for other

*Corresponding author. Tel.: +48 12 637 42 00; fax: +48 12 637 21 92.

E-mail addresses: annakor108@gmail.com, korneva_anna@mail.ru (A. Korneva).

ones the long-range mass transfer is needed. The results of such SPD-driven transitions cannot be explained by the bulk or even grain boundary diffusion at the SPD temperature (which usually remains slightly above ambient one). In this review the methods of T_{eff} determination of metallic alloys after high-pressure torsion are discussed. For the determination of T_{eff} we choose the alloys where the phases after HPT strongly differ from the ones before HPT. The alloys studied have also well investigated and unambiguously known equilibrium phase diagrams. These phase diagrams (in coordinates “temperature–composition” and/or “temperature–pressure”) allowed us the easy comparison with observed phases after SPD and, therefore, easy and reliable determination of T_{eff} .

2. Experimental

The Al–Zn, Al–Zn–Mg, Cu–Ni, Co–Cu, Ni–Y–Nb and Zr–Nb alloy systems of various compositions were investigated. The alloys were prepared of high purity components by the vacuum induction melting. The melts were poured in the vacuum into the water-cooled cylindrical copper crucible of 10 mm diameter. After sawing, grinding, and chemical etching, the 0.7 mm thick disks cut from the as cast cylinders were subjected to HPT in a Bridgman anvil type unit (room temperature, pressure 5 GPa, 5 torsions, 1 rotation-per-minute). After HPT, the central (low-deformed) part of each disk (about 3 mm in diameter) was excluded from further investigations. The samples for structural investigations and calorimetry were cut from the deformed disks at a distance of 4–5 mm from the sample centre. At this distance the shear strain is ~ 6 . The 2 mm thick slices were also cut from the cylindrical ingots, then divided into four parts. After quenching, samples were embedded in resin and then mechanically ground and polished, using 1 μm diamond paste in the last polishing step, for the metallographic study. After etching, samples were investigated by means of the light microscopy (LM) and by scanning electron microscopy (SEM). SEM investigations have been carried out in a Tescan Vega TS5130 MM microscope equipped with the LINK energy-dispersive spectrometer and on a Philips XL30 scanning microscope equipped with a LINK ISIS energy-dispersive spectrometer produced by Oxford Instruments. LM has been performed using a Neophot-32 light microscope equipped with a 10 Mpix Canon Digital Rebel XT camera. The samples for TEM investigations were prepared by ion milling on the PIPS machine. TEM investigations were carried out on a TECNAI F2 electron microscope with acceleration voltage of 200 kV. The dark field image was taken in the most bright reflection to which contribute both α and ω phases. X-ray diffraction (XRD) data were obtained on a Siemens diffractometer (CoK_{α} radiation). Grain size was estimated by the XRD line broadening and using the Scherer formula. Both the as-cast coarse-grained CG and fine-grained HPT-samples were studied with the aid of differential scanning calorimetry (DSC) using the NETZSCH Pegasus 404C and TA Instruments (models 910 and 1600) calorimeters in the dry argon atmosphere, Al_2O_3 crucibles and at the cooling and heating rates of 10 and 20 K/min.

3. Results and discussion

Usually, the high applied pressure decreases the diffusivity and grain boundary mobility [62,63]. However, the atom movements caused by strong external forces can drive both accelerated diffusion and phase transformations in the material [64]. Historically, such unusual behaviour was first observed in materials under severe irradiation [1]. Martin proposed a simplified mean-field description of solid solutions subjected to irradiation-induced atomic mixing [1]. His main idea was that the forced mixing induced by irradiation emulates the increase of entropy and changes the thermodynamic potentials in the alloy. In a simple case of regular solution in the Bragg–Williams approximation, a law of corresponding states was formulated: The equilibrium configuration of the solid under irradiation flux φ at temperature T is identical to the configuration at $\varphi=0$ and a certain effective temperature

$$T_{\text{eff}} = T(1 + \Delta). \quad (1)$$

If the irradiation-driven movements of atoms are similar in amplitude to conventional diffusion jumps, they can be described by the “ballistic” diffusion coefficient D_{ball} and $\Delta = D_{\text{ball}}/D_{\text{b}}$, where D_{b} is conventional bulk diffusion coefficient, possibly increased due to the non-equilibrium defect concentration [1]. It means that one can use the equilibrium phase diagram for the description of the system under irradiation, but at T_{eff} instead of the actual temperature T . For example, if the liquid phase is present in the phase diagram at T_{eff} , the amorphous phase would appear under irradiation [1,65].

To check the applicability of the Martin's law (1) to the forced diffusion driven by pure shear deformation (D_{HPT}) instead of irradiation (D_{ball}), experiments where HPT leads to the phase transformations have to be analysed. We have chosen for the comparison the data where (i) the HPT-driven atomic movements are comparable with each other, i.e. HPT was performed at 4–6 GPa with 4–6 torsions and (ii) the phases appeared after HPT can be easily localized in the phase diagrams and are different from those present in the samples before HPT.

The composition of the phases after SPD allows to localize those phases in the respective equilibrium phase diagram and to estimate the effective temperature T_{eff} . Such a schematic diagram is shown in Fig. 1. In this figure the dashed vertical lines denote compositions of the various studied alloys. Figurative points corresponding to the effective temperature of the alloys are indicated by an open circle and numbered. Each star with a letter indicates the composition and temperature of an alloy's treatment (normal cooling, SPD or rapid quenching).

The supersaturated solid solution in the as-cast Al–30 wt % Zn alloy contained about 15 wt% Zn (Fig. 2) [13,14,67]. It corresponds to the point *b* in Fig. 1. The as-cast Al–20 wt% Zn and Al–10 wt% Zn alloy contained about 7 and 3 wt% Zn in the supersaturated solid solution (Fig. 2). The HPT at room temperature (point *a* in Fig. 1) produced nanograined pure Al (point 1) and pure Zn particles simultaneously leading to unusual softening [13,14]. In other two as-cast alloys the

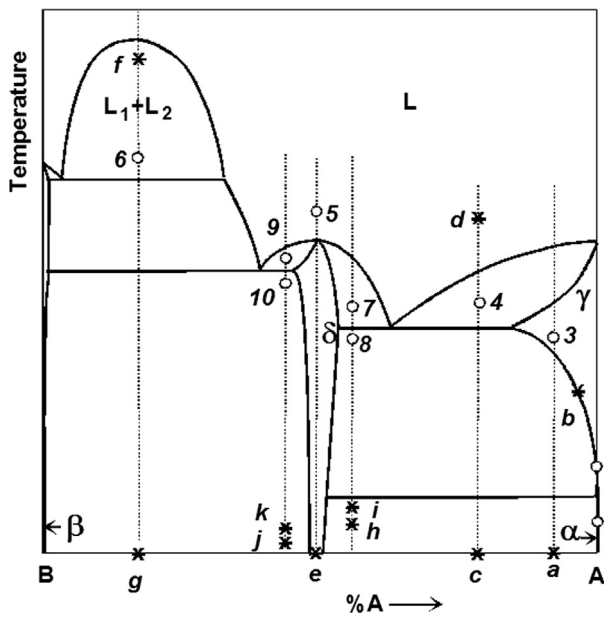


Fig. 1 - The schematic binary phase diagram showing the points of HPT deformation or other thermal treatments (stars) and respective configuration points at the (increased) effective temperatures. Other explanations are in the text.

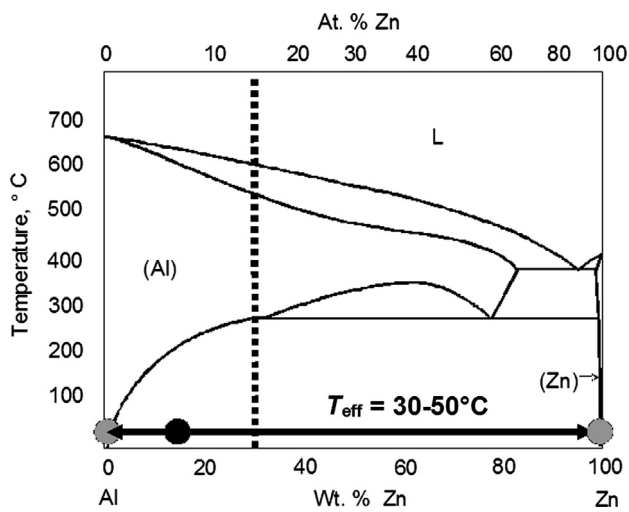


Fig. 2 - Al-Zn phase diagram [68]. Vertical dotted line shows the composition of Al-30 wt% Zn alloy. Large black circle shows the composition of supersaturated (Al) solid solution in coarse-grained Al-30 wt% Zn alloy before HPT. Large grey circles show the composition of phases in ultra-fine-grained Al-30 wt% Zn alloy after HPT [13]. The value of $T_{eff}=30-50\text{ }^{\circ}\text{C}$ is also given.

supersaturated solid solution also completely decomposed, and the lattice spacing in all three alloys became indistinguishable from that of pure aluminium (Fig. 3). The respective $T_{eff}=30\text{ }^{\circ}\text{C}$ (Fig. 2). The decomposition during SPD proceeds extremely quick, already after about 0.5 rotations of anvils the lattice spacing becomes equal to that of Al (Fig. 4) and microhardness reaches its stationary value (Fig. 5) [67].

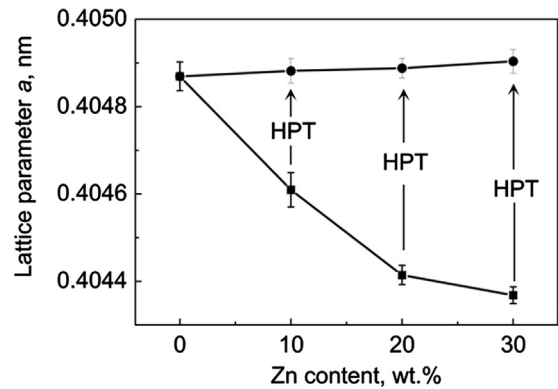


Fig. 3 - Dependence of the lattice parameter vs. the zinc concentration in the Al-Zn alloys before and after HPT [13].

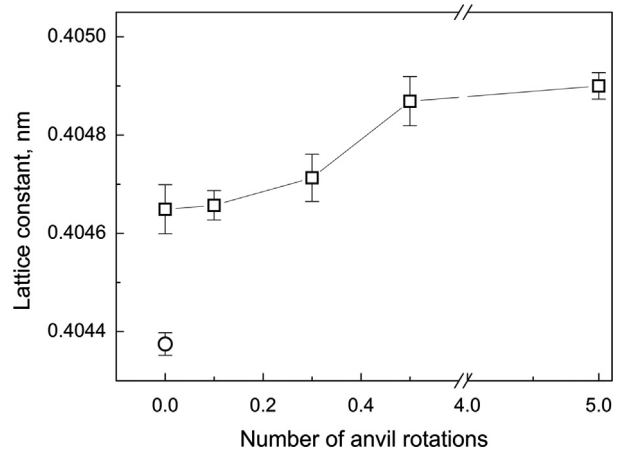


Fig. 4 - The dependence of the (Al) solid solution lattice parameter on the deformation degree [67].

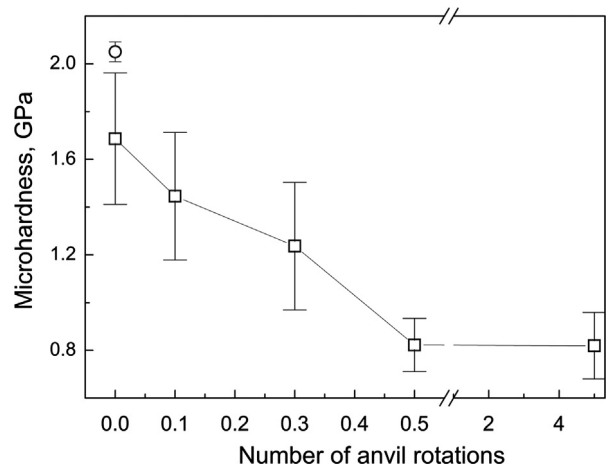


Fig. 5 - Dependence of microhardness of the Al-30% Zn alloy on the deformation degree [67].

The homogenized one-phase solid solutions in the Cu-Ni alloys with 42 and 77 wt% Ni (point 3) decomposed after HPT at room temperature (point a) into Cu-rich and Ni-rich phases (Fig. 6) [15]. The composition of resulting phases permitted an estimation of $T_{eff}=200\text{ }^{\circ}\text{C}$ for the Cu-77 mass% Ni alloy and $T_{eff}=270\text{ }^{\circ}\text{C}$ for the Cu-42 wt% Ni alloy (Fig. 6) [15].

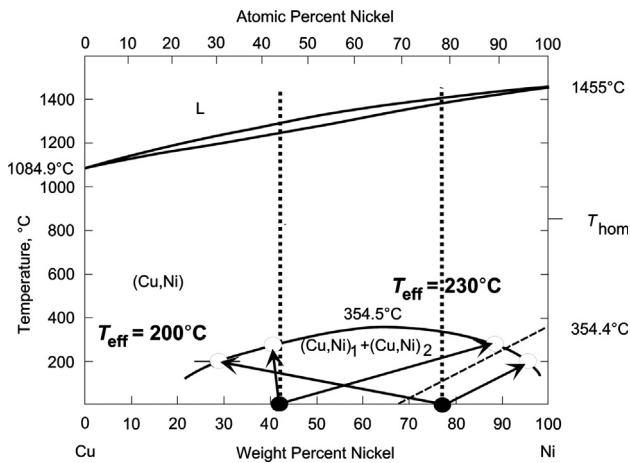


Fig. 6 – Cu–Ni phase diagram [67]. Vertical dotted lines show the composition of Cu–42 wt% Ni and Cu–77 wt% Ni alloys. Large black circles show the compositions of supersaturated (Cu) solid solutions in coarse-grained Cu–42 wt% Ni and Cu–77 wt% Ni alloys before HPT. They correspond with overall composition of both alloys. Large grey circles show the composition of phases in ultra-fine-grained Cu–42 wt% Ni and Cu–77 wt% Ni alloys after HPT [15]. The values of $T_{\text{eff}}=200^\circ\text{C}$ for the Cu–77 wt% Ni alloy and $T_{\text{eff}}=230^\circ\text{C}$ for the Cu–42 wt% Ni alloy are also given.

The results of the work on HPT of Co–Cu alloys are schematically shown by the points a, b and 2 (Fig. 1) [2]. The composition of the supersaturated solid solution of the component B in γ -phase of A corresponds to the point b. This undercooled supersaturated solid solution in the metastable γ -phase is HPT-treated in the point a. After HPT the almost pure α -phase of A is formed as a consequence of the γ - α transition. It corresponds to the point 2. In case of Co–Cu alloys, the as-cast Co–12 wtCu alloy contains the supersaturated solid solution with 8 wtCu in the Co matrix with fcc α -structure (Fig. 7). After HPT, together with grain refinement, the full decomposition of supersaturated (Co) solid solution proceeds. In addition, the high-temperature fcc α -Co transformed into low-temperature hcp ϵ -Co (Fig. 7). The respective $T_{\text{eff}}=400^\circ\text{C}$ for the Co–Cu system (Fig. 7) [2].

The Fe–20 wt% (Nd, Pr)–5 mass% B–1.5 wt% Cu alloy containing crystalline phases [(Nd,Pr)₂Fe₁₄B and Pr-rich phase] transforms after HPT (point c) into a mixture of the amorphous phase and (Nd,Pr)₂Fe₁₄B nanograins [16]. According to the Martin's model this means that the T_{eff} is so high that the configurative point for the treated alloy is in the two-phase area where both solid and liquid phases are present (point 4, Fig. 1). The melt appears in the Nd–Fe–B system above eutectic temperature $T_e=665^\circ\text{C}$ [17]. It means that the effective temperature is slightly above $T_e=665^\circ\text{C}$ and can be estimated as $T_{\text{eff}}=700^\circ\text{C}$.

The coarse-grained as-cast Ni–20 wt% Nb–30 wt% Y and Ni–18 wt% Nb–22 wt% Y alloys contained before HPT the NiY, NbNi₃, Ni₂Y, Ni₇Y₂ and Ni₃Y phases (point g, Fig. 1) (Fig. 8a) [36,39]. After HPT these alloys transformed into a mixture of two nanocrystalline NiY and Nb₁₅Ni₂ phases and two different amorphous phases (one was Y-rich and another Nb-rich) (point 6, Fig. 1). The Ni–Nb–Y phase diagram contains two immiscible

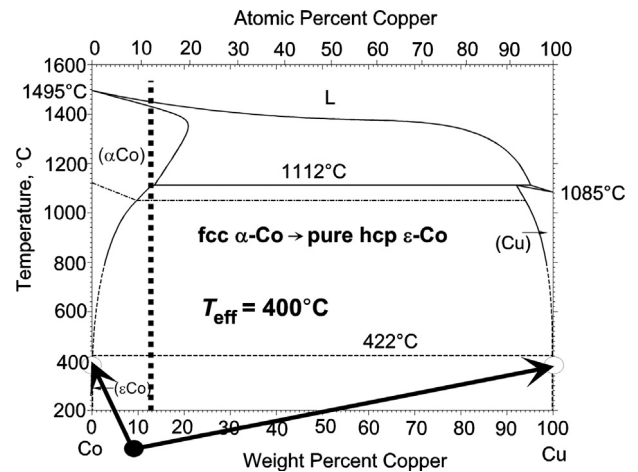


Fig. 7 – Co–Cu phase diagram [68]. Vertical dotted line shows the composition of Co–12 wt% Cu alloy. Large black circle shows the composition of supersaturated (Co) solid solution in coarse-grained Co–12 wt% Cu alloy before HPT. It contains fcc α -Co phase. Large grey circles show the composition of phases in ultra-fine-grained Co–12 wt% Cu alloy after HPT (pure hcp ϵ -Co and pure Cu) [2]. The value of $T_{\text{eff}}=400^\circ\text{C}$ is also given.

melts above 1440°C [66]. Therefore, the effective temperature is slightly above $T_e=1440^\circ\text{C}$ and can be estimated as $T_{\text{eff}}=1450^\circ\text{C}$ (Fig. 8b). It is remarkable that the rapid solidification of these alloys from the liquid state (point f, Fig. 1) also allows obtaining the mixture of two amorphous phases.

Especially valuable data on the effective temperature of SPD can be extracted from the work on HPT of Ti–48.5 at% Ni, Ti–50.0 at% Ni and Ti–50.7 at% Ni alloys [33]. The HPT of equiatomic Ti–50.0 at% Ni alloy at room temperature (point e, Fig. 1) resulted in the fully amorphous state (point 5, Fig. 1, $T_{\text{eff}}=1350^\circ\text{C}$, respectively). The HPT of the non-equiatomic Ti–48.5 at% Ni alloy at 270°C (point h) produced the mixture of amorphous and nanocrystalline phases (point 7, $T_{\text{eff}}=1050^\circ\text{C}$). When the HPT temperature of the Ti–48.5 at% Ni alloy increased up to 350°C (point i), only the mixture of nanocrystalline phases formed, without amorphous phase. It means that the corresponding point moved from the position 7 in the δ +L region into position 8 in the two-phase δ + γ region and the effective temperature decreased to $T_{\text{eff}}=950^\circ\text{C}$. The HPT of another non-equiatomic Ti–50.7 at% Ni alloy at 200°C (point j) produced the mixture of amorphous and nanocrystalline phases (point 9, $T_{\text{eff}}=1250^\circ\text{C}$). When the HPT temperature of the Ti–50.7 at% Ni alloy increased up to 250°C (point k), only the mixture of nanocrystalline phases formed, without amorphous phase. It means that the corresponding point moved from the position 9 in the δ +L region into position 10 in the two-phase δ + β region and the effective temperature decreased to $T_{\text{eff}}=1100^\circ\text{C}$. Therefore, it can be clearly seen from the data obtained by Prokoshkin et al. [33] that the increase of the HPT treatment temperature leads to the decrease of T_{eff} . It is in full accordance with Eq. (1) because the increase of T leads to increase of D_b , and at the same time the amount of deformation-driven atomic movements characterized by D_{HPT} remains unchanged.

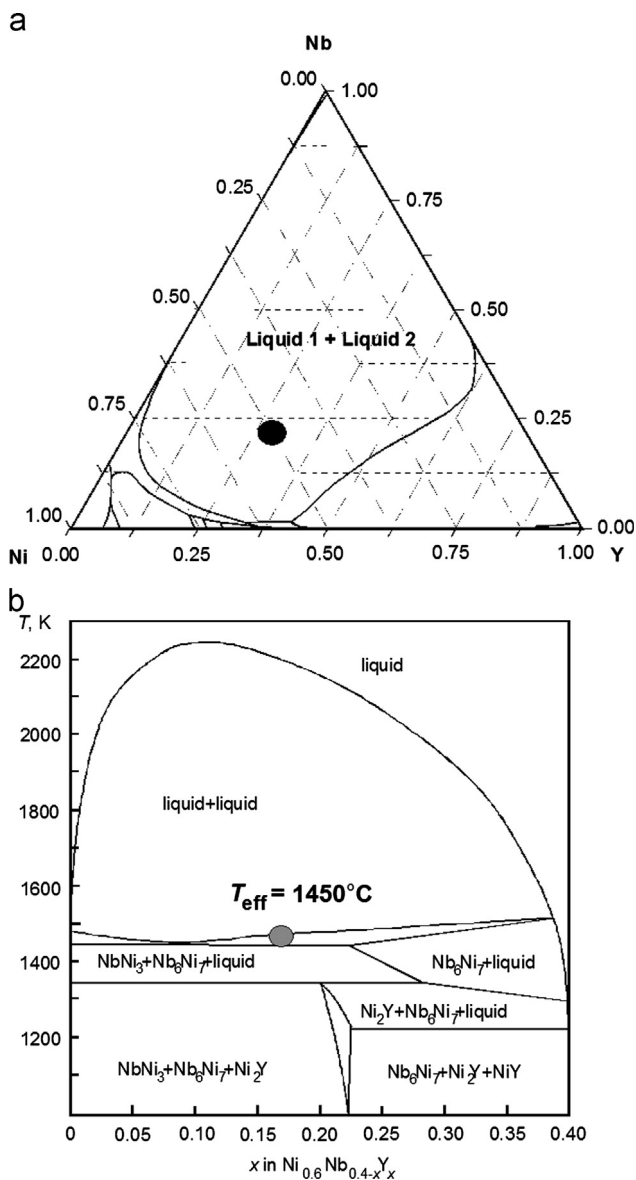


Fig. 8 – (a) Liquidus projection obtained by the CALPHAD method of the Y–Ni–Nb ternary phase diagram at [69]. The composition of the triple $Ni_{50}Nb_{20}Y_{30}$ alloy used for HPT investigations is marked by the large black circle. (b) Calculated pseudo-binary section of the ternary phase diagram $Ni_{60}Y_{40}$ – $Ni_{60}Nb_{40}$ [66]. Large grey circle shows the composition of phases in ultra-fine-grained alloy after HPT (two amorphous phases and two crystalline ones) [36,39]. The value of $T_{eff}=400$ °C is also given.

The values of T_{eff} can also be extracted from the experiments on the so-called nanocrystallization. The rapid solidification of these alloys from the liquid state (point d, Fig. 1) produces the fully amorphous phase. Afterwards the amorphous phase was subjected to the HPT at room temperature (point c, Fig. 1). HPT led to the formation of crystalline nanoparticles in the amorphous matrix (point 4, Fig. 1). The position of point 4 in a respective phase diagram slightly above the T_e permits to estimate T_{eff} . For the nanocrystallized Ni–29 wt% Fe–15 wt% Co–10 wt% B–2 wt% Si alloy [53] our

estimation gives $T_{eff}=1000$ °C. For the nanocrystallized Cu–20 wt% Zr–20 wt% Ti alloy [54] $T_{eff}=700$ °C. For the nanocrystallized Al–8 wt% Ce–5 wt% Ni–2 wt% Co alloy [55] $T_{eff}=400$ °C. For the nanocrystallized Fe–6 wt% Si–13 wt% B alloy [56] $T_{eff}=1100$ °C. For the nanocrystallized Zr–5 wt% Ti–20 wt% Cu–10 wt% Al–8 wt% Ni alloy [57] $T_{eff}=1100$ °C. We have to underline again that the effective temperatures determined in this way are much higher than the macroscopic temperature of the SPD-treatment which is usually only slightly above the ambient one. From this point of view HPT strongly differs for example from friction stir processing where the part being processed is really “lightening” during the treatment [70–72].

It is rather easy to estimate the T_{eff} if one can find the phases existing in a material before and after SPD in an equilibrium “temperature–composition” phase diagram. But it becomes a real challenge if the high-pressure phases appear during SPD. A good subject for such experiments is the titanium group of elements (Ti, Zr, and Hf). Ti, Zr, and Hf all have the hcp crystal structure (α -phase) at room temperature and zero pressure. At high temperature and zero pressure they transform to the bcc structure (β -phase) before reaching the melting temperature. At room temperature and under pressure they undergo a crystallographic phase change into the so-called ω -structure. At even higher pressures both Zr and Hf have been observed to transform to the bcc structure (β -phase) (see [73] and references therein).

The as-cast Zr–2.5 wt% Nb and Zr–8 wt% Nb alloys contain mainly α Zr with hexagonal closely-packed lattice [73]. The Nb-rich body-centred cubic phase is absent. Small amount of β -Zr is present in the CG as-cast alloys. Nb-poor β Zr has a body-centered cubic lattice and is isomorphous to the Nb-rich bcc-phase. After HPT both fine-grained Zr–Nb alloys contain mainly the ω -Zr phase [73]. The ω -Zr phase possesses the hexagonal C32 structure [74]. The Nb-rich (β -Nb-phase) is absent both after and before HPT. The HPT-treatment of Zr–2.5 wt% Nb and Zr–8 wt% Nb alloys at 5 GPa produced the ω -Zr high-pressure allotrope [73]. Therefore, the usage of equilibrium “temperature–composition” diagrams (like in Figs. 3, 6–8) is not enough to estimate the effective temperature of SPD. As we already mentioned above, high pressure always decreases the diffusivity and grain boundary mobility [62,63]. It means that in order to explain the increased atomic fluxes during SPD we need the increased T_{eff} , and we have to search for the respective phases in the “temperature–pressure” or even the “temperature–pressure–composition” phase diagrams.

In Fig. 9 the conditions of HPT (small full symbols) and the estimated values of effective temperatures (large open symbols) are shown for Ti, Zr and Hf. The starting α -phase in 99.8 wt% pure Zr [46] and commercially pure Zr [48] transforms into a ω + β mixture after HPT with 1 rpm and 5 rotations at 3 and 6 GPa (full squares, Fig. 7b) [46,48]. This fact permits to estimate the T_{eff} at the ω / β equilibrium line as 650 °C (open square). After HPT at 1 GPa [46,48,75], 2 GPa [46,50], 3 and 4 GPa [46] the α -phase does not transform in other phase(s). It does not permit to estimate the effective temperature of HPT process. The HPT at 6, 14, 22, 30 and 40 GPa with 1 rpm and 5 rotations (small full pentagons) transforms the starting α -phase into ω -phase [50,77].

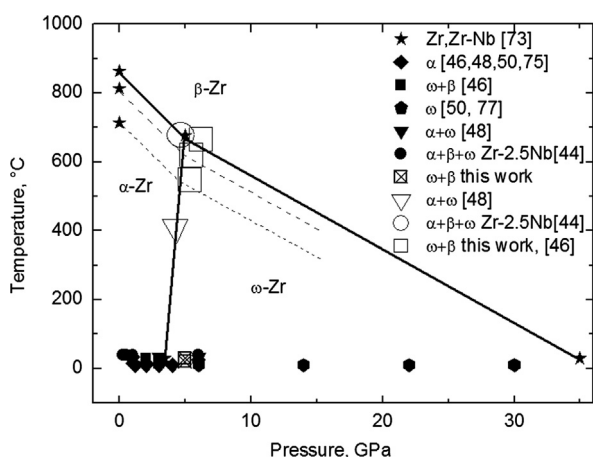


Fig. 9 – “Temperature–pressure” equilibrium phase diagram with data for HPT-experiments for zirconium [73]. Small full symbols mark the conditions of HPT-treatment and demonstrate the phases present in the samples after HPT. Large open symbols mark the effective temperatures in the respective phase fields. Diamonds are for the pure α -phase. Circles are for the $\alpha+\omega$ mixture. Triangles are for the $\alpha+\omega$ mixture. Squares are for the $\omega+\beta$ mixture. Hexagons are for the pure ω -phase.

However, the ω -phase is in equilibrium at room temperature above 3.4 GPa (star) [76]. Therefore, one cannot estimate the effective temperature using these results. The HPT of an Zr–2.5 wt% Nb alloy at 0.25, 0.5 and 5 GPa with 0.2 rpm and 5 rotations (full circles) permits to transform the starting α -phase into a $\alpha+\beta+\omega$ phase mixture [44]. This mixture can be found in the $\alpha+\beta+\omega$ triple point at 670 °C (large open circle). In our work the HPT of Zr–2.5 wt% Nb and Zr–8 wt% Nb finishes in the $\beta+\omega$ mixture, almost without any α -phase. Also, the addition of Nb decreases the temperature of α – β transition at ambient pressure (see also phase diagram in Fig. 3). One can suppose that the temperature of α – β (and ω – β) transition decreases in Zr–Nb alloys also at high pressures. The dashed lines starting in stars at 0.1 MPa show this shift for 2.5 and 8 wt% Nb. The respective effective temperatures are shown by large open squares and are $T_{\text{eff}}=620$ °C for Zr–2.5 wt% Nb and $T_{\text{eff}}=550$ °C for Zr–8 wt% Nb.

Analysing and comparing all these results, one can conclude that the original idea of Martin [1] is applicable, in its developed form, also to the SPD-driven phase transformations. We can draw this conclusion despite the fact that in the model of Martin it is supposed that the irradiation-driven movements of atoms are similar to the diffusion jumps. This is, obviously, not completely true for the case of SPD-driven movements of atoms. Nevertheless, the general tendency (1) is quite similar. In this work we have compared the alloys deformed by HPT in comparable conditions ($T_{\text{SPD}}\sim 300$ K, ~ 5 GPa, ~ 1 rpm, ~ 5 torsions) with each other. One can suppose that the SPD-driven atomic movements are comparable in all systems under consideration. On the other hand, the “natural” diffusion movements of the atoms are quite different due to the difference of melting temperature T_m of the considered materials. Since the $T_{\text{SPD}}\sim 300$ K is almost the

same, the “natural” diffusion coefficients are low for the materials with high T_m . In this case the SPD-driven atomic movements are large in comparison with diffusion jumps, and T_{eff} is high (as predicted by Martin, see Eq. (1)). In the opposite case of low T_m (like in the Al-based alloys), the T_{eff} is low and can be close to the ambient temperature of T_{SPD} [13,14,67].

4. Conclusions

Severe plastic deformation by HPT leads to the phase transitions and strong grain refinement in several metallic alloys. SPD-treatment at ambient temperature T_{SPD} is frequently equivalent to the heat treatment at a certain elevated (effective) temperature T_{eff} . If the condition of SPD-treatment is similar, the materials with high melting temperature T_m also yield high T_{eff} values. The materials with low T_m have low T_{eff} . Contrary to the effect of increasing temperature, the increasing pressure slows down the diffusion and grain boundary migration. Therefore, the forced atomic movement during HPT produces the states equivalent to higher temperature, but not to the higher pressure.

Acknowledgements

Authors thank the Russian Federal Ministry of Education and Science (Grant 14.A12.31.0001) and Polish National Science Centre (Grant DEC-2011/01/M/ST8/07822) for the financial support.

REFERENCES

- [1] G. Martin, Phase stability under irradiation: Ballistic effects, *Physical Review B* 30 (1984) 1424–1436.
- [2] B.B. Straumal, A.A. Mazilkin, B. Baretzky, E. Rabkin, R.Z. Valiev, Accelerated diffusion and phase transformations in Co–Cu alloys driven by the severe plastic deformation, *Materials Transactions* 53 (2012) 63–71.
- [3] X. Sauvage, A. Chbibi, X. Queleennec, Severe plastic deformation and phase transformations, *Journal of Physics* 240 (2010) 012003.
- [4] H.W. Zhang, S. Ohsaki, S. Mitao, A. Ohnuma, K. Hono, Microstructural investigation of white etching layer on pearlite steel rail, *Materials Science and Engineering: A* 421 (2006) 191–199.
- [5] W. Lojkowski, M. Djahanbakhsh, G. Burkle, S. Gierlotka, W. Zielinski, H.J. Fecht, *Materials Science and Engineering: A* 303 (2001) 197–208.
- [6] K. Hono, M. Ohnuma, M. Murayama, S. Nishida, A. Yoshie, T. Takahashi, Cementite decomposition in heavily drawn pearlite steel wire, *Scripta Materialia* 44 (2001) 977–983.
- [7] A. Taniyama, T. Takayama, M. Arai, T. Hamada, Structure analysis of ferrite in deformed pearlitic steel by means of X-ray diffraction method with synchrotron radiation, *Scripta Materialia* 51 (2004) 53–58.
- [8] V.G. Gavriljuk, Decomposition of cementite in pearlitic steel due to plastic deformation, *Materials Science and Engineering: A* 345 (2003) 81–89.
- [9] X. Sauvage, X. Queleennec, J.J. Malandain, P. Pareige, Nanostructure of a cold drawn tempered martensitic steel, *Scripta Materialia* 54 (2006) 1099–1103.
- [10] V.A. Teplov, V.P. Pilugin, V.S. Gaviko, E.G. Chernyshov, Nonequilibrium solid-solution and nanocrystal structure of

- Fe–Cu alloy after plastic deformation under pressure, *Philosophical Magazine: B* 68 (1993) 877–881.
- [11] V.V. Stolyarov, R. Lapovok, I.G. Brodova, P.F. Thomson, Ultrafine-grained Al–5 wt% Fe alloy processed by ECAP with backpressure, *Materials Science and Engineering: A* 357 (2003) 159–167.
- [12] X. Sauvage, F. Wetscher, P. Pareige, Mechanical alloying of Cu and Fe induced by severe plastic deformation of a Cu–Fe composite, *Acta Materialia* 53 (2005) 2127–2135.
- [13] B.B. Straumal, B. Baretzky, A.A. Mazilkin, F. Phillipp O.A. Kogtenkova, M.N. Volkov, R.Z. Valiev, Formation of nanograined structure and decomposition of supersaturated solid solution during high pressure torsion of Al–Zn and Al–Mg, *Acta Materialia* 52 (2004) 4469–4478.
- [14] A.A. Mazilkin, B.B. Straumal, E. Rabkin, B. Baretzky, S. Enders, S.G. Protasova, O.A. Kogtenkova, R.Z. Valiev, Softening of nanostructured Al–Zn and Al–Mg alloys after severe plastic deformation, *Acta Materialia* 54 (2006) 3933–3939.
- [15] B.B. Straumal, S.G. Protasova, A.A. Mazilkin, E. Rabkin D. Goll, G. Schütz, B. Baretzky, R.Z. Valiev, Deformation-driven formation of equilibrium phases in the Cu–Ni alloys, *Journal of Materials Science* 47 (2012) 360–367.
- [16] C.M. Cepeda-Jiménez, J.M. García-Infanta, A.P. Zhilyaev O.A. Ruano, F. Carreño, Influence of the thermal treatment on the deformation-induced precipitation of a hypoeutectic Al–7 wt% Si casting alloy deformed by high-pressure torsion, *Journal of Alloys and Compounds* 509 (2011) 636–643.
- [17] Y. Ivanisenko, I. MacLaren, X. Sauvage, R.Z. Valiev, H.-J. Fecht, Shear-induced $\alpha \rightarrow \gamma$ transformation in nanoscale Fe–C composite, *Acta Materialia* 54 (2006) 1659–1669.
- [18] X. Sauvage, Y. Ivanisenko, The role of carbon segregation on nanocrystallisation of pearlitic steels processed by severe plastic deformation, *Journal of Materials Science* 42 (2007) 1615–1621.
- [19] Y. Ivanisenko, W. Lojkowski, R.Z. Valiev, H.J. Fecht, The mechanism of formation of nanostructure and dissolution of cementite in a pearlitic steel during high pressure torsion, *Acta Materialia* 51 (2003) 5555–5570.
- [20] V.V. Sagaradze, S.V. Morozov, V.A. Shabashov L.N. Romashev, R.I. Kuznetsov, Solution of spherical and plate-like intermetallics in Fe–Ni–Ti austenitic alloys during cold working, *Physics of Metals and Metallography* 66 (1988) 328–338.
- [21] B.B. Straumal, A.A. Mazilkin, S.G. Protasova, S.V. Dobatkin A.O. Rodin, B. Baretzky, D. Goll, G. Schütz, Fe–C nanograined alloys obtained by high pressure torsion: structure and magnetic properties, *Materials Science and Engineering: A* 503 (2009) 185–189.
- [22] V.V. Sagaradze, V.A. Shabashov, Deformation-induced anomalous phase transformations in nanocrystalline FCC Fe–Ni based alloys, *Nanostructured Materials* 9 (1997) 681–684.
- [23] M. Murayama, K. Hono, Z. Horita, Microstructural evolution in an Al–1.7 at%Cu alloy deformed by equal-channel angular pressing, *Materials Transactions—JIM* 40 (1999) 938–941.
- [24] S. Ohsaki, S. Kato, N. Tsuji, T. Ohkubo, K. Hono, Bulk mechanical alloying of Cu–Ag and Cu/Zr two-phase microstructures by accumulative roll-bonding process, *Acta Materialia* 55 (2007) 2885–2895.
- [25] X. Sauvage, R. Pippa, Nanoscaled structure of a Cu–Fe composite processed by high-pressure torsion, *Materials Science and Engineering: A* 410–411 (2005) 345–347.
- [26] X. Sauvage, C. Genevois, G. Da Costa, V. Pantsyrny, Atomic scale characterization of deformation-induced interfacial mixing in a Cu/V nanocomposite wire, *Scripta Materialia* 61 (2009) 660–663.
- [27] X. Sauvage, W. Lefebvre, C. Genevois, S. Ohsaki, K. Hono, Complementary use of transmission electron microscopy and atom probe tomography for the investigation of steels nanostructured by severe plastic deformation, *Scripta Materialia* 60 (2009) 1056–1061.
- [28] B.B. Straumal, S.V. Dobatkin, A.O. Rodin, S.G. Protasova A.A. Mazilkin, D. Goll, B. Baretzky, Structure and properties of nanograined Fe–C alloys after severe plastic deformation, *Advanced Engineering Materials* 13 (2011) 463–469.
- [29] A.V. Korznikov, O. Dimitrov, G.F. Korznikova, J.P. Dallas A. Quivy, R.Z. Valiev, A. Mukherjee, Nanocrystalline structure and phase transformation of the intermetallic compound TiAl processed by severe plastic deformation, *Nanostructured Materials* 11 (1999) 17–23.
- [30] A.V. Korznikov, G. Tram, O. Dimitrov, G.F. Korznikova S.R. Idrisova, Z. Pakiel, The mechanism of nanocrystalline structure formation in Ni₃Al during severe plastic deformation, *Acta Materialia* 49 (2001) 663–671.
- [31] C. Rentenberger, H.P. Karnthaler, Extensive disordering in long-range-ordered Cu₃Au induced by severe plastic deformation studied by transmission electron microscopy, *Acta Materialia* 56 (2008) 2526–2530.
- [32] A.V. Sergueeva, C. Song, R.Z. Valiev, A.K. Mukherjee, Structure and properties of amorphous and nanocrystalline NiTi prepared by severe plastic deformation and annealing, *Materials Science and Engineering: A* 339 (2003) 159–165.
- [33] S.D. Prokoshkin, I.Yu. Khmelevskaya, S.V. Dobatkin I.B. Trubitsyna, E.V. Tatyannin, V.V. Stolyarov, E.A. Prokofiev, Alloy composition, deformation temperature, pressure and post-deformation annealing effects in severely deformed Ti–Ni based shape memory alloys, *Acta Materialia* 53 (2005) 2703–2714.
- [34] X. Sauvage, L. Renaud, B. Deconihout, D. Blavette, D.H. Ping, K. Hono, Solid state amorphization in cold drawn Cu/Nb wires, *Acta Materialia* 49 (2001) 389–394.
- [35] T. Miyazaki, D. Terada, Y. Miyajima, C. Suryanarayana R. Murao, Y. Yokoyama, K. Sugiyama, M. Umemoto, T. Todaka, N. Tsuji, Synthesis of non-equilibrium phases in immiscible metals mechanically mixed by high pressure torsion, *Journal of Materials Science* 46 (2011) 4296–4301.
- [36] A.A. Mazilkin, G.E. Abrosimova, S.G. Protasova, B.B. Straumal, G. Schütz, S.V. Dobatkin, A.S. Bakai, Transmission electron microscopy investigation of boundaries between amorphous “grains” in Ni₅₀Nb₂₀Y₃₀ alloy, *Journal of Materials Science* 46 (2011) 4336–4342.
- [37] V.V. Stolyarov, D.V. Gunderov, A.G. Popov, V.S. Gaviko A.S. Ermolenko, Structure evolution and changes in magnetic properties of severe plastic deformed Nd(Pr)–Fe–B alloys during annealing, *Journal of Alloys and Compounds* 281 (1998) 69–71.
- [38] Y. Matsuura, S. Hirose, H. Yamamoto, S. Fujimira M. Sagawa, K. Osamura, Phase diagram of the Nd–Fe–B ternary system, *Japanese Journal of Applied Physics. Part 2—Letters* 24 (1985) L635–L637.
- [39] B.B. Straumal, A.A. Mazilkin, S.G. Protasova, D. Goll B. Baretzky, A.S. Bakai, S.V. Dobatkin, Formation of two amorphous phases in the Ni₆₀Nb₁₈Y₂₂ alloy after high pressure torsion, *Kovove Materialy—Metallic Materials* 49 (2011) 17–22.
- [40] Á. Révész, S. Hóbor, J.L. Lábár, A.P. Zhilyaev, Zs. Kovács, Partial amorphization of a Cu–Zr–Ti alloy by high pressure torsion, *Journal of Applied Physics* 100 (2006) 103522.
- [41] I. MacLaren, Y. Ivanisenko, R.Z. Valiev, H.J. Fecht, Reverse martensitic transformation of ferrite to austenite under severe plastic deformation, *Journal of Physics* 26 (2006) 335–338.
- [42] Y. Ivanisenko, I. MacLaren, X. Sauvage, R.Z. Valiev, H.J. Fecht, Phase transformations in pearlitic steels induced by severe plastic deformation, *Solid State Phenomena* 114 (2006) 133–144.

- [43] Y. Ivanisenko, I. MacLaren, X. Sauvage, R.Z. Valiev, H.J. Fecht, Shear-induced $\alpha \rightarrow \gamma$ transformation in nanoscale Fe–C composite, *Acta Materialia* 54 (2006) 1659–1669.
- [44] A.P. Zhilyaev, I. Sabirov, G. González-Doncel, J. Molina-Aldareguía, B. Srinivasarao, M.T. Pérez-Prado, Effect of Nb additions on the microstructure, thermal stability and mechanical behavior of high pressure Zr phases under ambient conditions, *Materials Science and Engineering: A* 528 (2011) 3496–3505.
- [45] A.P. Zhilyaev, A.V. Sharafutdinov, M.T. Pérez-Prado, Phase transformations during high-pressure torsion of pure Zr and of a Zr-2.5%Nb alloy, *Advanced Engineering Materials* 12 (2010) 754–757.
- [46] A.P. Zhilyaev, F. Gálvezc, A.V. Sharafutdinov, M.T. Pérez-Prado, Influence of the high pressure torsion die geometry on the allotropic phase transformations in pure Zr, *Materials Science and Engineering: A* 527 (2010) 3918–3928.
- [47] M.T. Pérez-Prado, A.V. Sharafutdinov, A.P. Zhilyaev, Thermal stability of pure bcc Zr fabricated by high pressure torsion, *Materials Letters* 64 (2010) 211–214.
- [48] M.T. Pérez-Prado, A.P. Zhilyaev, First experimental observation of shear induced hcp to bcc transformation in pure Zr, *Physical Review Letters* 102 (2009) 175504.
- [49] K. Edalati, Z. Horita, Y. Mine, High-pressure torsion of hafnium, *Materials Science and Engineering: A* 527 (2010) 2136–2141.
- [50] K. Edalati, Z. Horita, S. Yagi, E. Matsubara, Allotropic phase transformation of pure zirconium by high-pressure torsion, *Materials Science and Engineering: A* 523 (2009) 277–281.
- [51] K. Edalati, E. Matsubara, Z. Horita, Processing pure Ti by high-pressure torsion in wide ranges of pressures and strain, *Metallurgical and Materials Transactions A* 40 (2009) 2079–2086.
- [52] Y. Ivanisenko, A. Kilmametov, H. Roesner, R.Z. Valiev, Evidence of $\alpha \rightarrow \omega$ phase transition in titanium after high pressure torsion, *International Journal of Materials Research* 99 (2008) 36–41.
- [53] A.M. Glezer, M.R. Plotnikova, A.V. Shalimova, S.V. Dobatkin, Severe plastic deformation of amorphous alloys: I. Structure and mechanical properties, *Bulletin of the Russian Academy of Sciences: Physics* 73 (2009) 1233–1236.
- [54] S. Hóbor, Á. Révész, A.P. Zhilyaev, Zs. Kovács, Different nanocrystallization sequence during high pressure torsion and thermal treatments of amorphous $\text{Cu}_{60}\text{Zr}_{20}\text{Ti}_{20}$ alloy, *Reviews on Advanced Materials Science* 18 (2008) 590–592.
- [55] Zs. Kovács, P. Henits, A.P. Zhilyaev, Á. Révész, Deformation induced primary crystallization in a thermally non-primary crystallizing amorphous $\text{Al}_{85}\text{Ce}_8\text{Ni}_5\text{Co}_2$ alloy, *Scripta Materialia* 54 (2006) 1733–1737.
- [56] G.E. Abrosimova, A.S. Aronin, S.V. Dobatkin, S.D. Kaloshkin, D.V. Matveev, O.G. Rybchenko, E.V. Tatyannin, I.I. Zverkova, The formation of nanocrystalline structure in amorphous Fe–Si–B alloy by severe plastic deformation, *Journal of Metastable and Nanocrystalline Materials* 24 (2005) 69–72.
- [57] Á. Révész, E. Schafler, Zs. Kovács, Structural anisotropy in a $\text{Zr}_{57}\text{Ti}_5\text{Cu}_{20}\text{Al}_{10}\text{Ni}_8$ bulk metallic glass deformed by high pressure torsion at room temperature, *Applied Physics Letters* 92 (2008) 011910.
- [58] S. Hóbor, Zs. Kovács, A.P. Zhilyaev, L.K. Varga, P.J. Szabó, Á. Révész, High pressure torsion of Cu-based metallic glasses, *Journal of Physics* 240 (2010) 012153.
- [59] S. Hóbor, Á. Révész, P.J. Szabó, A.P. Zhilyaev, V. Kovács Kis J.L. Lábár, Zs. Kovács, High pressure torsion of amorphous $\text{Cu}_{60}\text{Zr}_{30}\text{Ti}_{10}$ alloy, *Journal of Applied Physics* 104 (2008) 033525.
- [60] P. Henits, Á. Révész, A.P. Zhilyaev, Zs. Kovács, Severe plastic deformation induced nanocrystallization of melt-spun $\text{Al}_{85}\text{Y}_8\text{Ni}_5\text{Co}_2$ amorphous alloy, *Journal of Alloys and Compounds* 461 (2008) 195–199.
- [61] Zs. Kovács, P. Henits, A.P. Zhilyaev, N.Q. Chinh, Á. Révész, Microstructural characterization of the crystallization sequence of a severe plastically deformed Al–Ce–Ni–Co amorphous alloy, *Materials Science Forum* 519–521 (2006) 1329–1334.
- [62] B.B. Straumal, L.M. Klinger, L.S. Shvindlerman, The influence of pressure on indium diffusion along single tin–germanium interphase boundaries, *Scripta Metallurgica* 17 (1983) 275–279.
- [63] D.A. Molodov, B.B. Straumal, L.S. Shvindlerman, The effect of pressure on migration of the [001] tilt grain boundaries in the tin bicrystals, *Scripta Metallurgica* 18 (1984) 207–211.
- [64] B.B. Straumal, A.S. Gornakova, Y.O. Kucheev, B. Baretzky, A. N. Nekrasov, Grain boundary wetting by a second solid phase in the Zr–Nb alloys, *Journal of Materials Engineering and Performance* 21 (2012) 721–724.
- [65] G. Thomas, H. Mori, H. Fujita, Electron irradiation induced crystalline amorphous transitions in Ni–Ti alloys, *Scripta Metallurgica* 16 (1982) 589–592.
- [66] N. Mattern, U. Kühn, A. Gebert, A. Schoeps, T. Gemminga L. Schultz, Phase separation in liquid and amorphous Ni–Nb–Y alloys, *Materials Science and Engineering: A* 449/451 (2007) 207–210.
- [67] A.A. Mazilkin, B.B. Straumal, M.V. Borodachenkova, R.Z. Valiev, O.A. Kogtenkova, B. Baretzky, Gradual softening of Al–Zn alloys during high pressure torsion, *Materials Letters* 84 (2012) 63–65.
- [68] T.B. Massalski (Ed.), *Binary Alloy Phase Diagrams*, 2nd ed., ASM International, Materials Park, OH, 1990.
- [69] U.R. Kattner, The thermodynamic modeling of multicomponent phase equilibria, *JOM* 49 (12) (1997) 14–19.
- [70] S. Swaminathan, K. Oh-Ishi, A.P. Zhilyaev, Ch.B. Fuller B. London, M.W. Mahoney, T.R. McNelley, Peak stir zone temperatures during friction stir processing, *Metallurgical and Materials Transactions A* 41 (2010) 631–640.
- [71] T. Giles, K. Oh-Ishi, A.P. Zhilyaev, S. Swaminathan M.W. Mahoney, T.R. McNelley, The effect of friction stir processing on the microstructure and mechanical properties of an aluminum lithium alloy, *Metallurgical and Materials Transactions A* 40 (2009) 104–115.
- [72] K. Oh-Ishi, A.P. Zhilyaev, T.R. McNelley, A microtexture investigation of recrystallization during friction stir processing of as-cast NiAl bronze, *Metallurgical and Materials Transactions A* 37 (2006) 2239–2251.
- [73] B.B. Straumal, A.S. Gornakova, O.B. Fabrichnaya, M.J. Kriegel, A.A. Mazilkin, B. Baretzky, A.M. Gusak, S.V. Dobatkin, Effective temperature of high pressure torsion in Zr–Nb alloys, *High Temperature Material Processes* 31 (2012) 339–350.
- [74] S.K. Sikka, Y.K. Vohra, R. Chidambaram, Omega phase in materials, *Progress in Materials Science* 27 (1982) 245–310.
- [75] A.V. Sergueeva, V.V. Stolyarov, R.Z. Valiev, A.K. Mukherjee, Advanced mechanical properties of pure titanium with ultrafine grained structure, *Scripta Materialia* 45 (2001) 747–752.
- [76] J. Zhang, Y. Zhao, P.A. Rigg, R.S. Hixson, G.T. Gray III, Impurity effects on the phase transformations and equations of state of zirconium metals, *Journal of Physics and Chemistry of Solids* 68 (2007) 2297–2302.
- [77] M.T. Pérez-Prado, A.A. Gimazov, O.A. Ruano, M.E. Kassner, A.P. Zhilyaev, Bulk nanocrystalline ω -Zr by high-pressure torsion, *Scripta Materialia* 58 (2008) 219–222.